

Biophysical Journal, Volume 113

Supplemental Information

Computational Lipidomics of the Neuronal Plasma Membrane

Helgi I. Ingólfsson, Timothy S. Carpenter, Harsh Bhatia, Peer-Timo Bremer, Siewert J. Marrink, and Felice C. Lightstone

Supporting Material for:

Computational lipidomics of the neuronal plasma membrane

Helgi I. Ingólfsson, Timothy S. Carpenter, Harsh Bhatia, Peer-Timo Bremer, Siewert J.

Marrink, and Felice C. Lightstone

Supplementary Methods

Lipid compositions

For the composition of the **Average** plasma membrane (PM) we used the idealized mammalian PM mixture described in (1). The **Average** mixture is composed of 63 different Martini lipid types asymmetrically distributed between the outer and inner membrane leaflets (Figure 1A). Different regions within the brain, and different cell types can have diverse membrane compositions (2-4). However, properly isolating large numbers of specific cell types can be extremely difficult. Thus, given the type of neural lipidomic data available, it was more sensible to construct a model that possessed the general properties of membranes found within the brain. The **Brain** composition represents the lipid composition of human brain tissue or more specifically a typical human neuronal PM mixture. The lipid compositions between different tissue types can vary greatly (5, 6) but specific numbers are hard to determine as a cell membrane lipid compositions can vary with cell type, age, diet, environment and disease state (5, 7-12). To capture a **Brain** PM composition, we did not base our composition on a single brain lipidomic study but a consensus from a number of studies (6, 13-24), and how those vary compared to the **Average** mixture. An overview of the **Brain** and the **Average** compositions is given in Figure 1. The specific lipid types used, their ratio in the outer/inner leaflets, and the lipid counts in the simulations are listed in Table S1. The average percentages of the main headgroup types were adjusted to match average consensus values from (13, 14, 16, 17, 21-24). The main differences being that the **Brain** has a significantly higher cholesterol content. The **Brain** mixture also has less PC and more PE. The **Brain** has less SM but includes cerebroside that are not present in the **Average** model. PIPs and PI lipids can be hard to resolve in lipidomic studies (25, 26) and were kept at similar concentration as in the **Average** mixture. Additionally, the tail length distributions and tail saturation was adjusted based on reported distribution of PC, PE and SM lipids in (6, 18, 20, 21) as well as overall saturated, monounsaturated, and polyunsaturated distributions from (6, 20).

Force fields

The Martini coarse-grain (CG) model (27, 28) was used for all simulations and all the lipid force fields used can be found at the Martini portal (www.cgmartini.nl). The newest available lipid model was used in all cases except where indicated. New lipid parameters were constructed according to the standard Martini 2.0 lipid building blocks and rules (27, 28) as detailed in (1, 29) using the *lipid-martini-itp-v06.py*; available at the at the Martini portal. The names as well as the Martini CG tail bead composition of all the lipids used in the average mammalian plasma membrane (**Average**) and average neuronal plasma membrane (**Brain**) can be found in Table S1. The Martini O tail, representing oleic acid or palmitoleic acid, was recently updated to CDCC (29) instead of the CCDC used in (1). The **Average** mixture is used unmodified from (1) and therefore has the old arrangement, but the new arrangement was tested for the **Average** mixture in the control simulation **Average new all**. The linker for the lyso lipids has also been updated and, similarly, the old arrangement was kept in in the **Average** mixture but the new one used for the **Brain** mixture and the **Average new all** control simulation. The Martini diacylglycerol (DAG) lipids have recently been updated; the GL1 bead type changed from Nda to P1 to better represent the polarity of the glycerol. This change affects the flip-flop rate of the DAG lipids. For direct comparison of the flip-flop rates the old DAG parameters were used in the main simulations but a control simulation with the new parameters was done (**Average new all**). A modified version of the Martini GM1 and GM3 parameters were recently published that better match the size of ganglioside clusters seen with the GROMOS atomistic force field (30). The original GM1/GM3 parameters (1, 31) were used in the main simulations but the modified parameters were tested in a few control simulations (**Average new all**, **Average new GM**, and **Brain new GM**). The cerebroside lipids in the average neuronal plasma membrane (**Brain**) are modeled by the Martini GS headgroup, a general model for glucosylceramide and galactosylceramide (31).

Detailed simulation set up

The simulations were run using the GROMACS 4.6.7 simulation package (32) using the standard Martini parameters set; called *common* in (33). The simulations were set up following the same protocol as described in (1). In short, the initial configuration of each membrane was set up using the bilayer builder *insane* (29). Each system was energy-minimized (steepest descent, 1500 steps) and simulated for 0.5 ns using a short time step of 10 fs, followed by production runs using a time step of 20 fs. In the production runs large membrane undulations were restricted using weak position restraints ($2 \text{ kJ mol}^{-1} \text{ nm}^{-2}$) on the PO4 bead Z-direction of DPPC, POPC and PIPC lipids in the outer leaflet; see Ingólfsson *et al.* (1) supplementary information for control simulations exploring the effects of these restraints. To explore the effects of undulations simulations with no restraints and weaker restraints ($0.2 \text{ kJ mol}^{-1} \text{ nm}^{-2}$) were also run. The number of lipids in the outer/inner leaflet of each bilayer mixture was adjusted based on independent $1 \mu\text{s}$ long simulation with symmetrical composition of each leaflet. In these simulations bilayer undulations were suppressed to get better estimates of the average area per

lipid without undulations; this was done by imposing the same *Z*-directional position restraints as above but with a force constant of $100 \text{ kJ mol}^{-1} \text{ nm}^{-2}$. The cholesterol distribution between the outer/inner leaflet was equilibrated using the same protocol as described in (1). The initial mixture was started with 50/50 cholesterol distribution: average area per lipid was measured in a pair of symmetrical outer/inner mixture simulations; asymmetrical simulations setup with adjusted number of lipids in either leaflet; the cholesterol distribution was allowed to equilibrate for a few μs ; cholesterol leaflet distribution was measured and used as the new initial values for the next round of simulations. This process was iterated until the initial cholesterol concentration was stable.

The final lipid numbers for the large ($\sim 20,000$ lipids) **Average** and **Brain** simulations are listed in Table S1. The smaller ($\sim 6,000$ lipids) control simulations have the same relative lipid ratios as the larger simulations. Additionally, the simulations include counter ions, 150 mM NaCl, and $\sim 300,000$ Martini water molecules for the larger simulations and $\sim 100,000$ for the smaller. The simulations were run at 310 K, with $\tau_T = 1.0 \text{ ps}$, controlled with the velocity rescaling thermostat (34) and at 1 bar semi-isotropic pressure, with $\tau_p = 5.0 \text{ ps}$, controlled using the Parrinello-Rahman barostat (35). The larger simulations were run for 80 μs and the smaller control simulations for 50 μs . Additionally, simulations with no or weaker undulation restraints were run for 5 μs starting from the larger simulations at 75 μs .

All simulation times reported are actual times simulated and were not scaled. CG models have less degrees of freedom compared to their atomistic counterparts and therefore normally less friction which leads to overall faster dynamics. The effective speedup varies depending on the molecule and system in question but for Martini the speedup is often pegged at around 4-fold (28).

Analysis

The average area per lipid (A_l) of the outer and inner leaflet of the **Average** and **Brain** lipid mixtures were estimated individually in simulations of symmetric bilayers containing 6,000-7,000 lipids of the outer or the inner lipid mixtures. The simulations were kept flat using strong position restraints, force constant $100 \text{ kJ mol}^{-1} \text{ nm}^{-2}$ (see above) and simulated for 1 μs . The A_l was estimated as the average box area of the last 100 ns divided by the number of lipids in each leaflet; resulting in outer/inner A_l of 0.513 / 0.553 and 0.460 / 0.485 nm^2 for the **Average** and **Brain**, respectively, with standard error $\sim 0.001 \text{ nm}^2$.

A lipid flip-flop is defined when a lipid moves from one leaflet to another and flip-flop rates were measured as described in (1). The **Brain** membrane thickness fluctuates somewhat more than the **Average** membrane, therefore, we extended the cutoff length for what is considered within a leaflet to 1.1 nm removing spurious flip-flop event. Lipid flip-flop rates were calculated for all lipid classes and averaged over the last 10 μs of the simulations. During the simulations, only the CHOL, DAG and ceramide (CER) lipid types flip-flopped. The measured flip-flop rates per molecule are: CHOL $7.290 \pm 0.018 \times 10^6 \text{ s}^{-1}$, DAG $7.662 \pm 0.049 \times 10^6 \text{ s}^{-1}$, and

CER $2.7 \pm 0.6 \times 10^4 \text{ s}^{-1}$ and CHOL $4.820 \pm 0.004 \times 10^6 \text{ s}^{-1}$, DAG $2.800 \pm 0.074 \times 10^6 \text{ s}^{-1}$, and CER $1.5 \pm 0.5 \times 10^4 \text{ s}^{-1}$ for the **Average** and **Brain** membranes, respectively. The error is estimated as the standard error of the mean when the last 10 μs of the simulations were split in three equally sized blocks and analyzed separately. Flip-flop rates for the alternative parameter control simulations are given in the legend of Figure S7.

Cholesterol fraction in the bilayer middle was determined by counting the number of cholesterols whose ROH bead was within 0.8 nm of the bilayer center averaged over the last 10 μs of the simulations.

In order to explore undulation in lipid bilayers, we project the headgroups on an approximate surface representing the bilayer membrane, and compute properties, such as area per lipid, curvature, and normals on these projections. In particular, given the positions of the headgroups, P_i , the undulations in bilayers can be captured using the following steps:

1. The lipid bilayer leaflets were defined using the MDAnalysis leaflet finder (36). The top headgroup bead was used for all lipids, except for the Glyco, PI and PIP lipids; where the GM1 and C1 beads were used. Initially, the outer and inner leaflets were defined from all non-flip-flopping lipids, then for each simulation frame the flip-flopping lipids with headgroup beads within 1.2 nm of either leaflet were included in those leaflets.
2. Surface fitting requires consistently oriented normal vectors n_i for each P_i . Normals are computed using the principal component analysis (PCA) in the local neighborhood around P_i , and oriented consistently through a depth-first traversal of the distance-based minimum spanning tree of P_i (37). Finally, using the Poisson reconstruction method (38) on (P_i, n_i) , an approximate surface, Ψ , is obtained as a representative of the bilayer membrane. The Poisson reconstruction is a global solution, and is chosen because it provides a natural way to smooth noisy fluctuations in the given points, while maintaining the overall shape of the surface.
3. The obtained surface, Ψ , is then projected onto the 2D Euclidean plane, giving Ψ° using discrete harmonic mapping (39), which allows keeping the angular distortion to a minimum. The given positions of the headgroups, P_i , are then projected on Ψ , giving P_i^Ψ . Using the surface projection obtained above, these points are then projected to the 2D plane, giving P_i° . Using two projections, i.e., $P_i \rightarrow P_i^\Psi \rightarrow P_i^\circ$ allows minimizing distortion to the curvature and area per lipid, and thus, provides better approximation of the said properties, as compared to directly projecting the points onto the 2D plane.
4. A periodic 2D Delaunay triangulation is then performed on P_i° , which establishes a neighborhood graph, \mathcal{T} between P_i° , and hence, P_i . Given the connectivity \mathcal{T} on the original points P_i^Ψ , we compute bilayer normals, N_i . Note that, using the triangulation enables a more accurate estimation of bilayer normals as compared to those computed in Step 2. Finally, we quantify the undulations in bilayers as the angle between the bilayer normal N_i and upward z-axis, i.e., $b_i = \cos^{-1}(|N_i^z|)$.

Lipid tail order was evaluated using the lipid tail order parameter (S), defined as:

$$S = \frac{1}{2} (3 \langle (\cos \theta)^2 \rangle - 1).$$

where θ is the angle between the vector along a particular lipid tail bond and the bilayer normal at the given lipid. The bilayer normal, N_i , is defined from the bilayer surface as described above. Tail order was evaluated for each lipid tail of each lipid type separately for the outer and inner leaflets, except for DAG and CER lipids that flip-flop between the leaflets. The absolute average order parameter of a particular lipid tail up to the lipids linker (AM or GL beads) was used for comparing the different tails overall order/flexibility, see Table S2. The weighted average order parameters (excluding lipids that flip-flop) are: **Average** [0.435,0.374] / [0.430,0.301] and **Brain** [0.487,0.391] / [0.444,0.224], respectively for the [sn-1, sn-2] tails in the outer/inner leaflet. For both the **Average** and **Brain** membranes the inner leaflet tails are less ordered than the outer leaflet but the difference is significantly greater in the **Brain** membrane. The increased tail order (excluding DAG and CER lipids) in the outer with respect to the inner is 11% for the **Average** and 31% for the **Brain**. The lipid tail lengths vary between the different lipid types, therefore, we also evaluated the tail order using S at pos3 (between beads 2 and 3, present in all non-sterol lipids). Combining the lipid tails and calculating the weighted average between all lipids at pos3 the order in the outer/inner leaflet is: **Average** 0.412/0.349 and **Brain** 0.445/0.301, with a weighted error of ~ 0.001 or less. That is an increase of 18% and 48% for the outer over the inner leaflet of the **Average** and **Brain** membranes, respectively.

The lipid lateral diffusion coefficients (D) were calculated from the mean square displacement (MSD) of the molecules in each membrane plane. The GROMACS `g_msd` tool was used over the last 10 μ s of the simulations to obtain the diffusion coefficients and errors. The MSD curves, excluding the first and last 10% of each curve, were fitted to $y = 4Dt + c$, to obtain D . For each lipid type the GL1, AM1 or ROH bead was used for the glycerol, ceramide or cholesterol lipids, respectively. All diffusion values are reported in Table S3. Note, lipid diffusion coefficients are reported as is and no correction is applied for overestimates due to the larger effective simulation speed of CG simulations (28) or underestimates due to the periodically bound finite system sizes (40).

Lipid neighbor counting was used to evaluate non-ideal lipid mixing, Figure S2. Lipids in the same leaflet and within a 1.5 nm radius XY plane cut-off were considered as neighbors, values were averaged over the last 10 μ s of the simulations and their relative enrichment/depletion compared to random mixing, see detailed description of method in (1).

For an indicator of overall lipid mobility lipid root mean square fluctuations (RMSF) over the last 2 μ s were used (Figure S3A and B). RMSF were calculated for all non-flip-flopping lipids based on their GL1 or AM1 beads using the GROMACS `g_rmsf` tool and plotted onto of their corresponding beads at 80 μ s.

Bilayer thickness plots were created by calculating the local average distance in the Z-direction between the phosphate beads (PO4) and the first headgroup bead of the glycolipids (GM1 or C1) in the two leaflets, averaged over the last 2 μ s the simulations, and plotted using the tool `g_thickness` (41). The plot was subsequently drawn using bins of 1.42 x 1.42 nm and a

color scale varying from 3.6 to 4.4 nm (Figure S3C). Average bilayer thickness was determined in five blocks over the last 10 μ s the simulations resulting in 4.109 ± 0.001 nm for the **Average** and 4.057 ± 0.002 for the **Brain**.

Lipid flow analysis was carried out on the last 2 μ s of the simulations using the methodology described by Chavent *et al.* (42). The trajectories were firstly pre-processed to remove the center of mass motion and subjected to low-pass filtering to remove high frequency noise using the GROMACS `g_filter` function. The filtering of the systems was carried out over a time scale of 200 ns. The leaflet correlation function, $C_l(t)$, at time t , as taken from Chavent *et al.* (42), defined as:

$$C_l(t) = \frac{1}{N} \sum_{i=1}^N \frac{\vec{u}_{i(t)} \cdot \vec{v}_{i(t)}}{|\vec{u}_{i(t)}| |\vec{v}_{i(t)}|}$$

The system is divided into a grid of cells, where N is the number of non-empty cells in the grid, and \cdot denotes the scalar product of vectors $u_{i(t)}$ and $v_{i(t)}$ as defined as the distance between the center of mass of the constituent lipids at time $t+dt$ and at time t . $u_{i(t)}$ and $v_{i(t)}$ are the lower and upper leaflet vectors.

Lipid clustering based on cholesterol density. To define lipid domains a kernel density estimator was used to define a cholesterol density. After several experiments with different kernel bandwidths a Gaussian kernel $K(x,y) = \exp(-\|x-y\| / s^2)$ with $s = 3$ nm was chosen as a good balance between smoothing local variations and detecting small, transient domains. Given the density value at each cholesterol a periodic Delaunay triangulation was computed using the CGAL library (Computational Geometry Algorithms Library, www.cgal.org). Finally, domains for high/low cholesterol were defined using density thresholds. More specifically, regions of high cholesterol were defined as connected components of the Delaunay triangulation above a given threshold and regions of low cholesterol symmetrically as connected components below a given threshold. To efficiently explore the impact of different threshold choices the topological analysis framework described in (43, 44) was used to encode all domains for all possible thresholds in form of a so called merge-/split-tree. This is equivalent to a traditional isosurface extraction but computationally more efficient. Domain size was defined as the number of cholesterol part of each lipid domain.

The cross-correlations between the cholesterol density of the outer/inner leaflet was calculated for every 5 ns of the simulations. The cholesterol densities were resampled to a 128x128 pixel grid and the Pearson correlation calculated between the leaflets, Figure 3C. Average values over the last 10 μ s of the simulations are 0.45 ± 0.01 and -0.14 ± 0.01 for the **Average** and **Brain** mixtures, respectively, where the error was estimated by splitting the last 10 μ s into four equal parts and calculating the standard error between the averages of the parts.

Density maps were calculated in the bilayer XY-plane, with a bin size of ~ 2 nm. One bead per lipid was used, as indicated, and averaged over the last 2 μ s of the simulations.

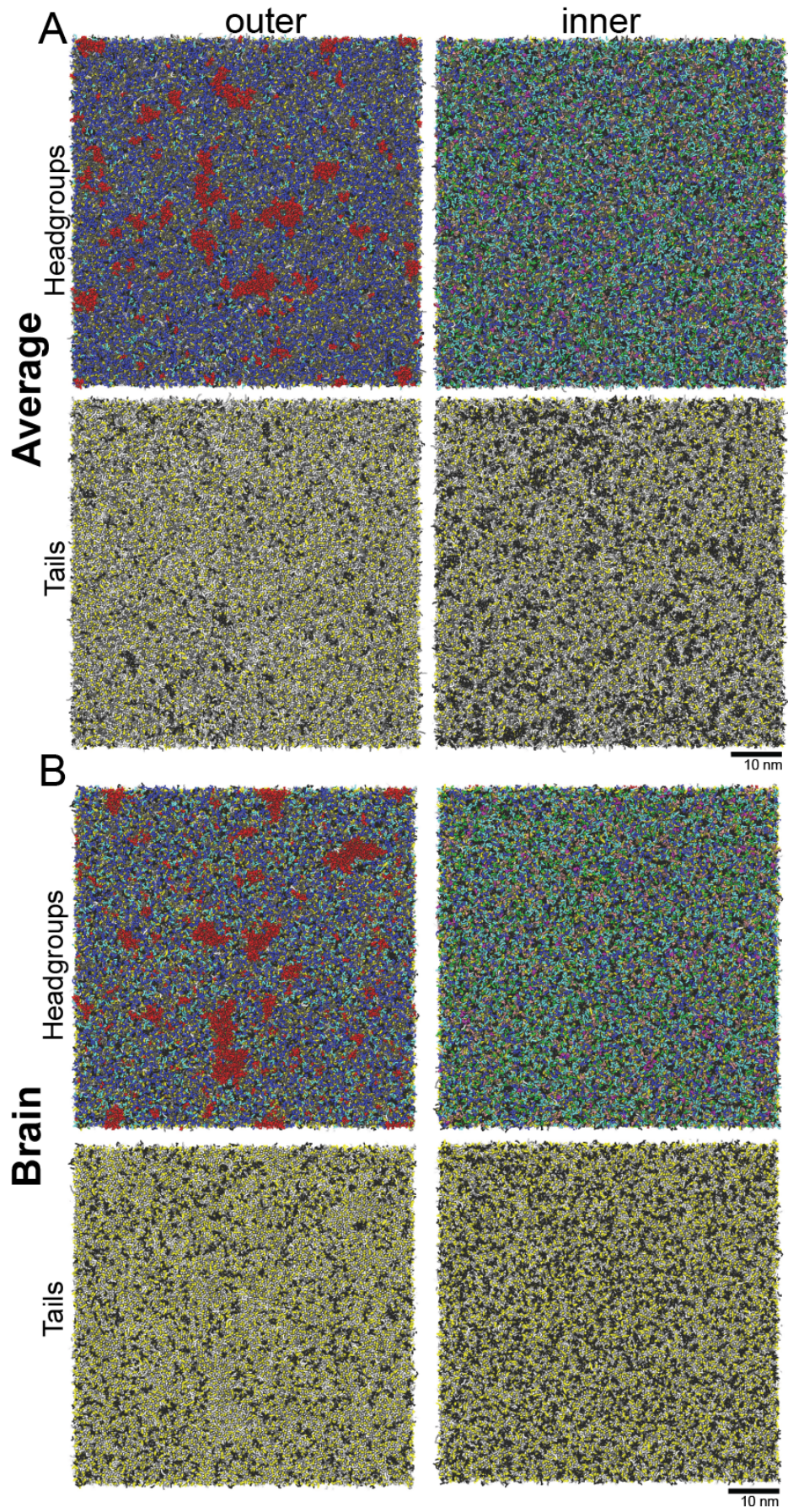


Figure S1. Lipid headgroup and tail configuration. Snapshots of the outer/inner leaflets of the **Average** (A) and **Brain** (B) mixtures after 80 μ s of simulation. The snapshots are shown with the headgroups and without to illustrating the tails; the color scheme for the lipid headgroups and tails is the same as used in Fig. 1. The lipids are colored by type (PC, blue; SM, gray; PE, cyan; Glyco, red; PIPs, magenta; PI, pink; PS, green; PA, white; CE, ice blue; DG, brown; LPC, orange; CHOL, yellow,) and tails by number of saturations (0, white; 1, light gray; 2, dark gray; 3-6, black) and cholesterol shown in yellow.

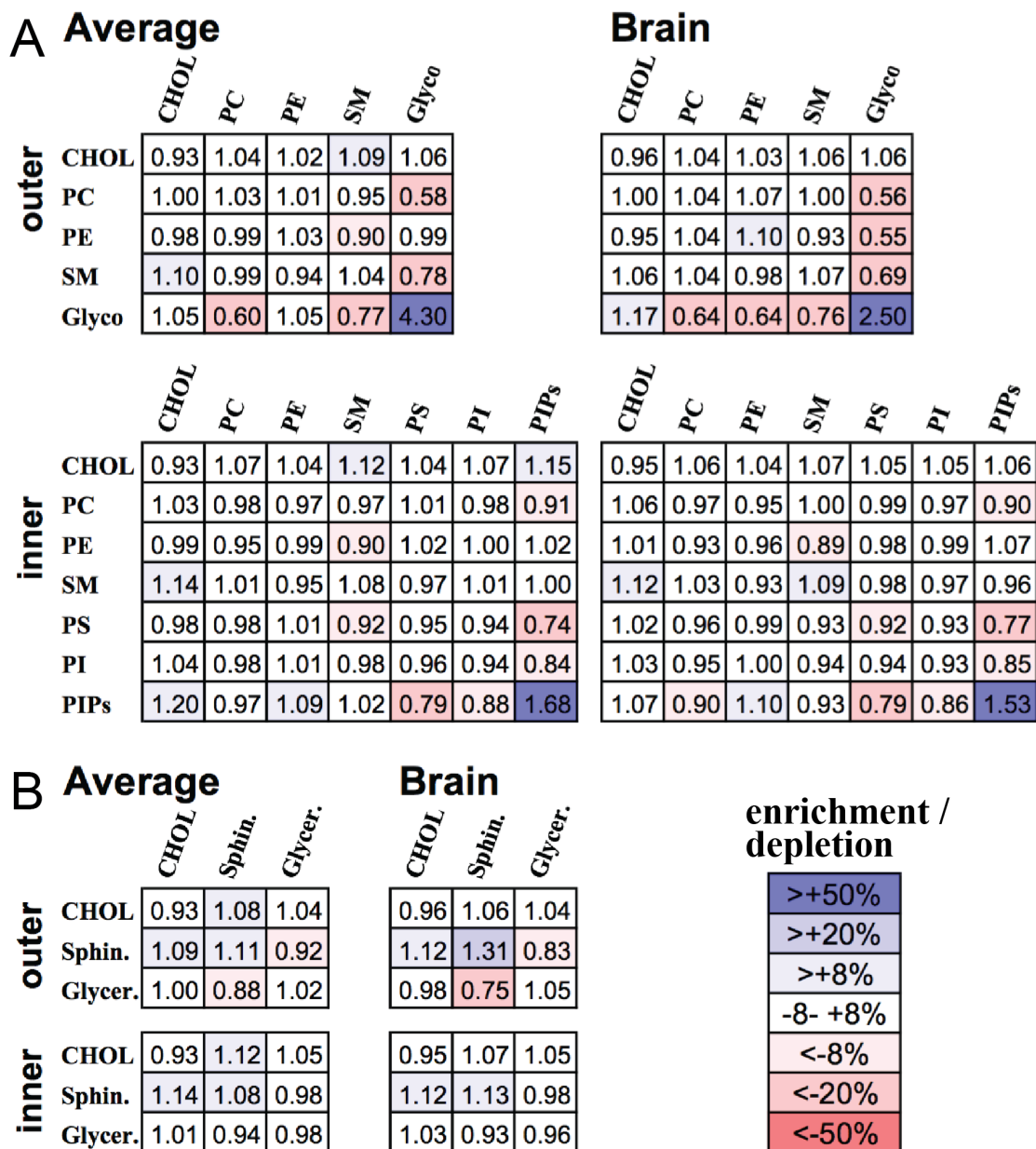


Figure S2. Non-ideal lipid mixing. Number of neighboring lipids (within 1.5 nm) grouped by headgroup type (A) and linker type (B); where Sphin. are sphingolipids and Glycer. are glycerolipids. Values are averaged over the last 10 μ s of the simulation and normalized to the weighted average number of neighbors of each type to highlight the relative enrichment/depletion of those lipids. Standard errors for all counts are <0.03 .

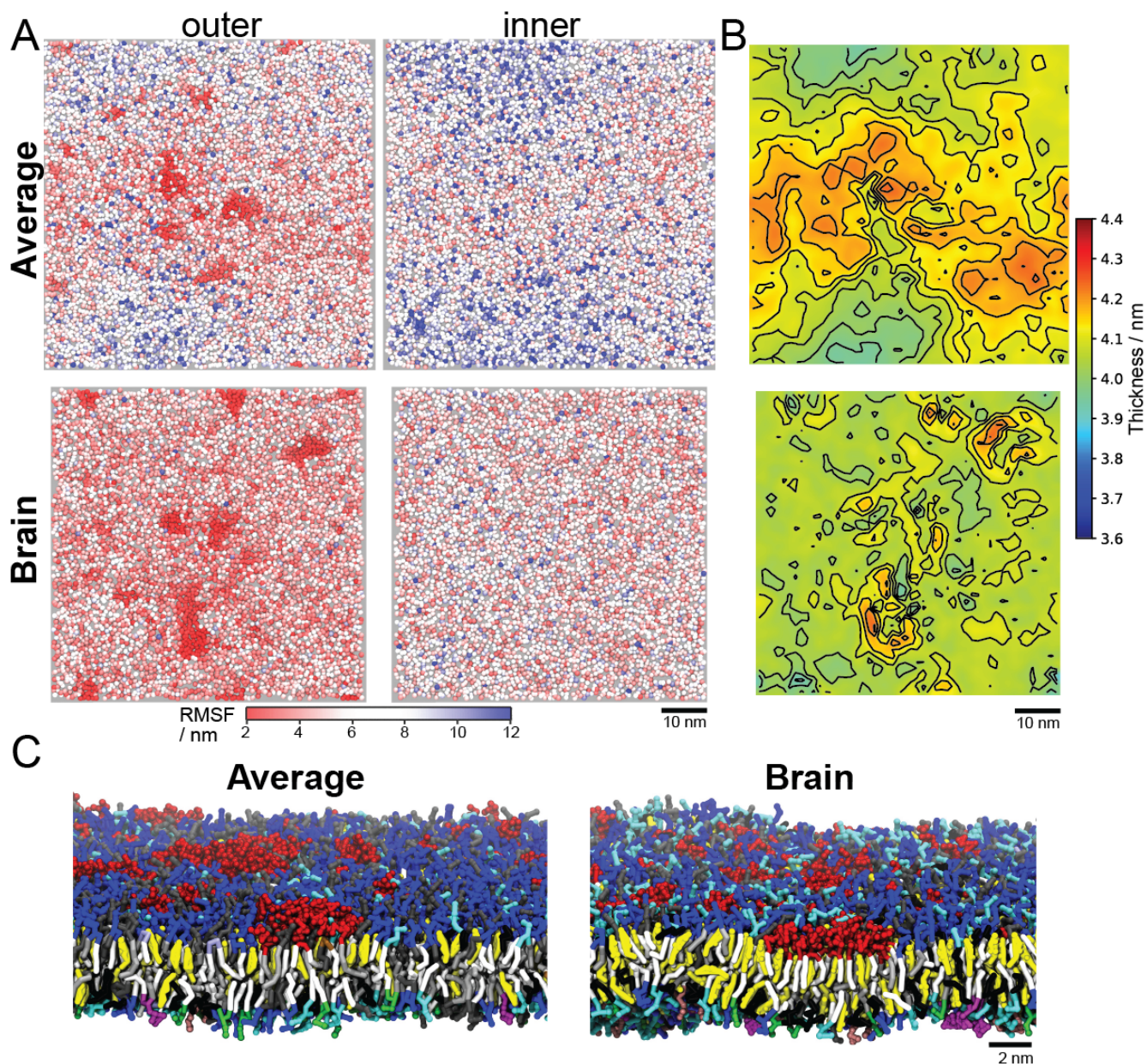


Figure S3. Membrane domain properties. (A) PM lipid root mean square fluctuations (RMSF) are shown to indicate differences in lipid mobility. RMSF values were calculated for the GL1 and AM1 linker beads of all non-flip-flopping lipids over the last 2 μ s of the simulations and plotted onto the bead positions at 80 μ s. Note, the dark red clusters in the outer leaflets of both the **Average** and **Brain** corresponds to clusters of glycolipids. (B) 2D PM thickness plots, calculated between all PO4 beads in either leaflets. The average thickness is similar between the PMs (4.11 nm for the **Average** and 4.06 nm for the **Brain**). (C) Representative zoomed in snapshots for the **Average** and **Brain** PM side and outer leaflet. The lipids are colored in the same way as in Fig. 1. Somewhat tighter packing and more local undulations can be seen in the **Brain** mixture, despite same method for reducing large undulations.

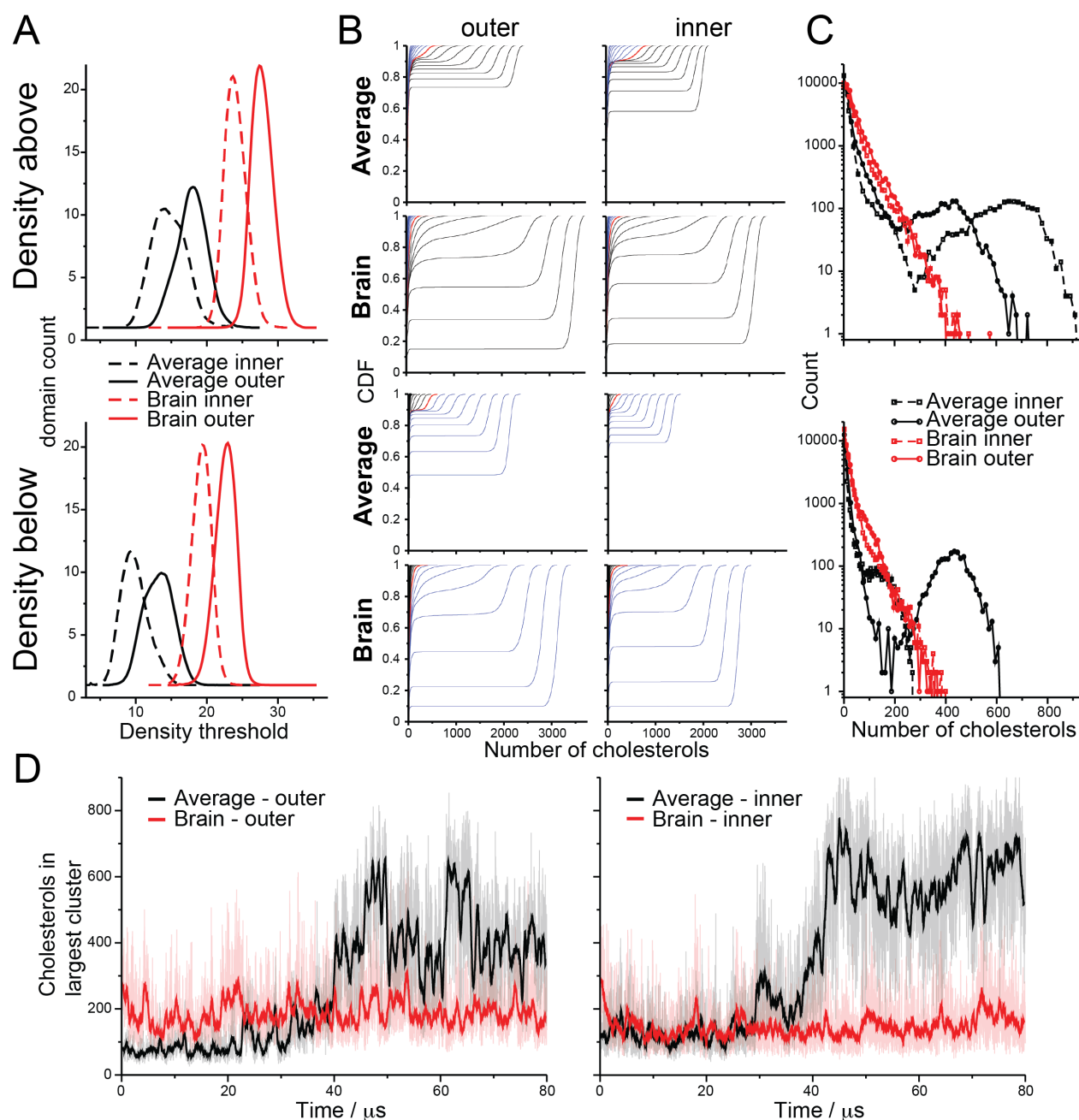


Figure S4. Cholesterol density cluster parameter sensitivity. (A) For the outer (solid lines) and inner (dotted lines) leaflets of the **Average** (black) and **Brain** (red) membranes the average number of domains per frame were computed over the last 10 μs for a range of possible thresholds. The top panel is numbers with higher density than specified (high-density regions) and the bottom panels is lower density than specified (low-density regions). (B) The cumulative distribution function (CDF) of domain “sizes” (number of cholesterol) for a range of thresholds. The selected threshold (max of A) is shown in red: [18.1, 13.6] / [14.0, 9.4] and [27.4, 23.0] / [23.7, 19.4] for the **Average** and **Brain** [high, low] outer/inner, respectively. Additionally, x8 lower thresholds in blue and x8 higher thresholds in black are shown; deviating from the selected threshold in 0.5 increments. (C) Histograms of the domain sizes (in number of cholesterol) at the selected threshold. (A-C) Are averaged over the last 10 μs of the simulations. (D) Size (in

number of cholesterols) of the largest high-density domain in each frame of the **Average** and **Brain** simulations. Shown for every 5 ns (dimmed lines) and average over 500 ns (bold lines).

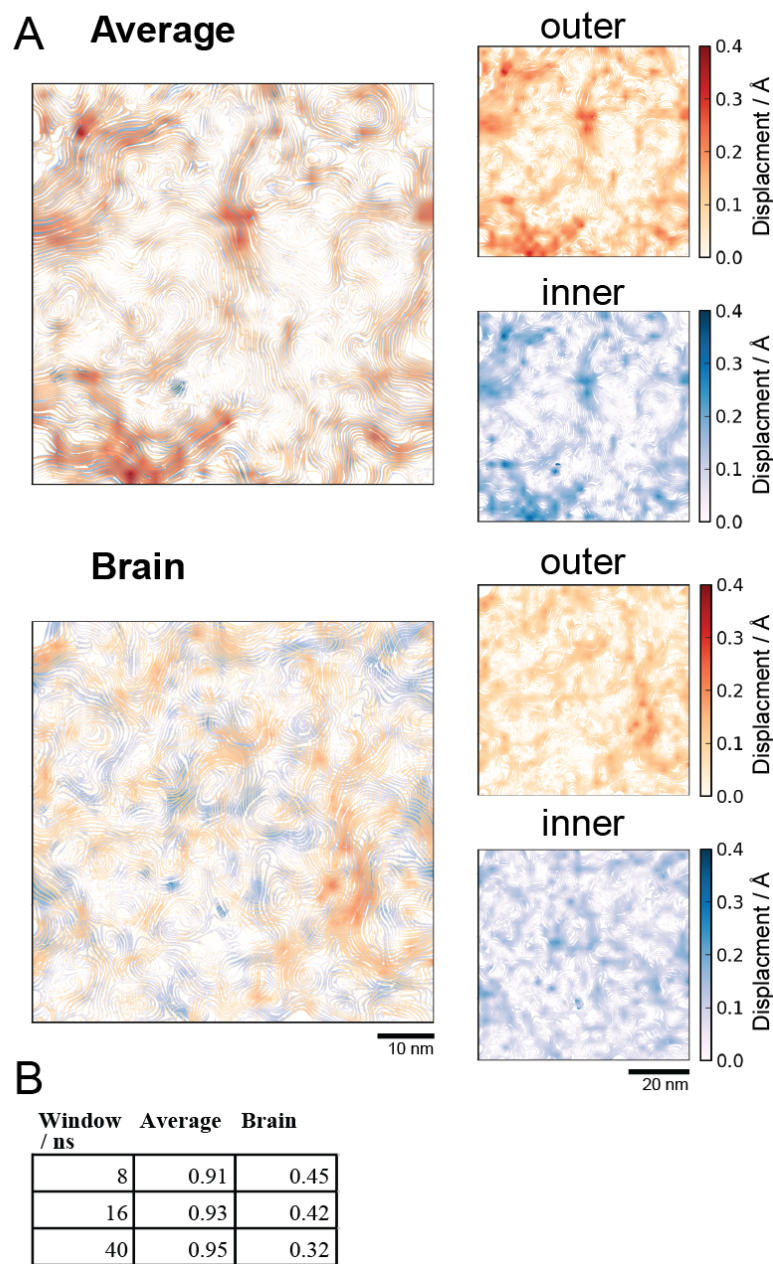


Figure S5. Lipid flow analysis. (A) Using sampling over the final 200 ns of each PM simulation, the mean-squared displacement for each lipid leaflet is calculated and tracked using the *flow* methodology (see SI Methods). The average displacement is shown for both the outer (red scale) and inner (blue scale) leaflets separately in the smaller images, and are overlaid together in the larger images to highlight correlations in regions of similar displacement. (B) The inter-leaflet lipid flow correlation is shown as a function temporal smoothing window (ns) to illustrate that the lipid flow of the **Average** PM mixture is highly correlated but the **Brain** mixture not so much, especially over longer timescales.

Figure S6A-B

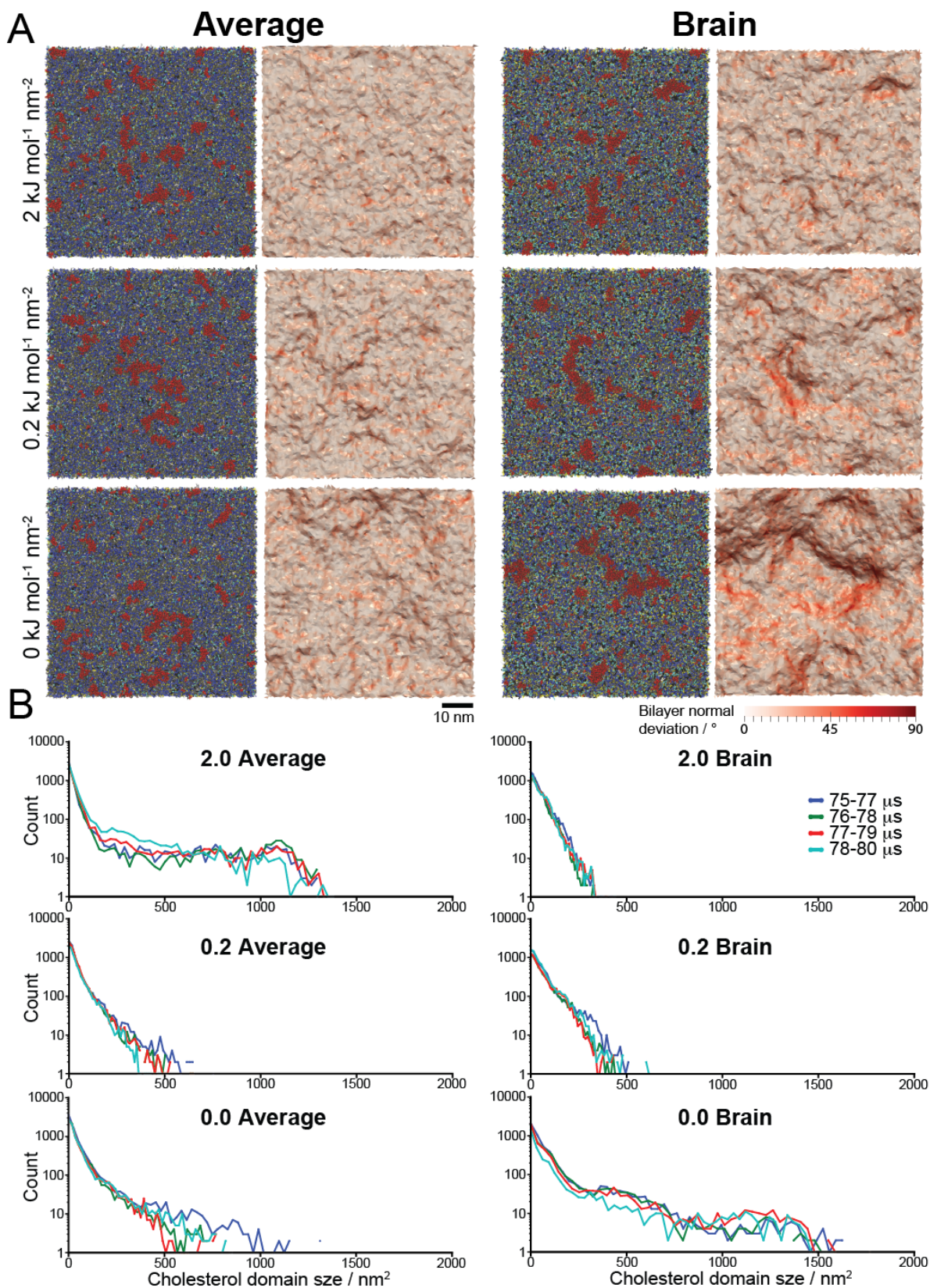


Figure S6C

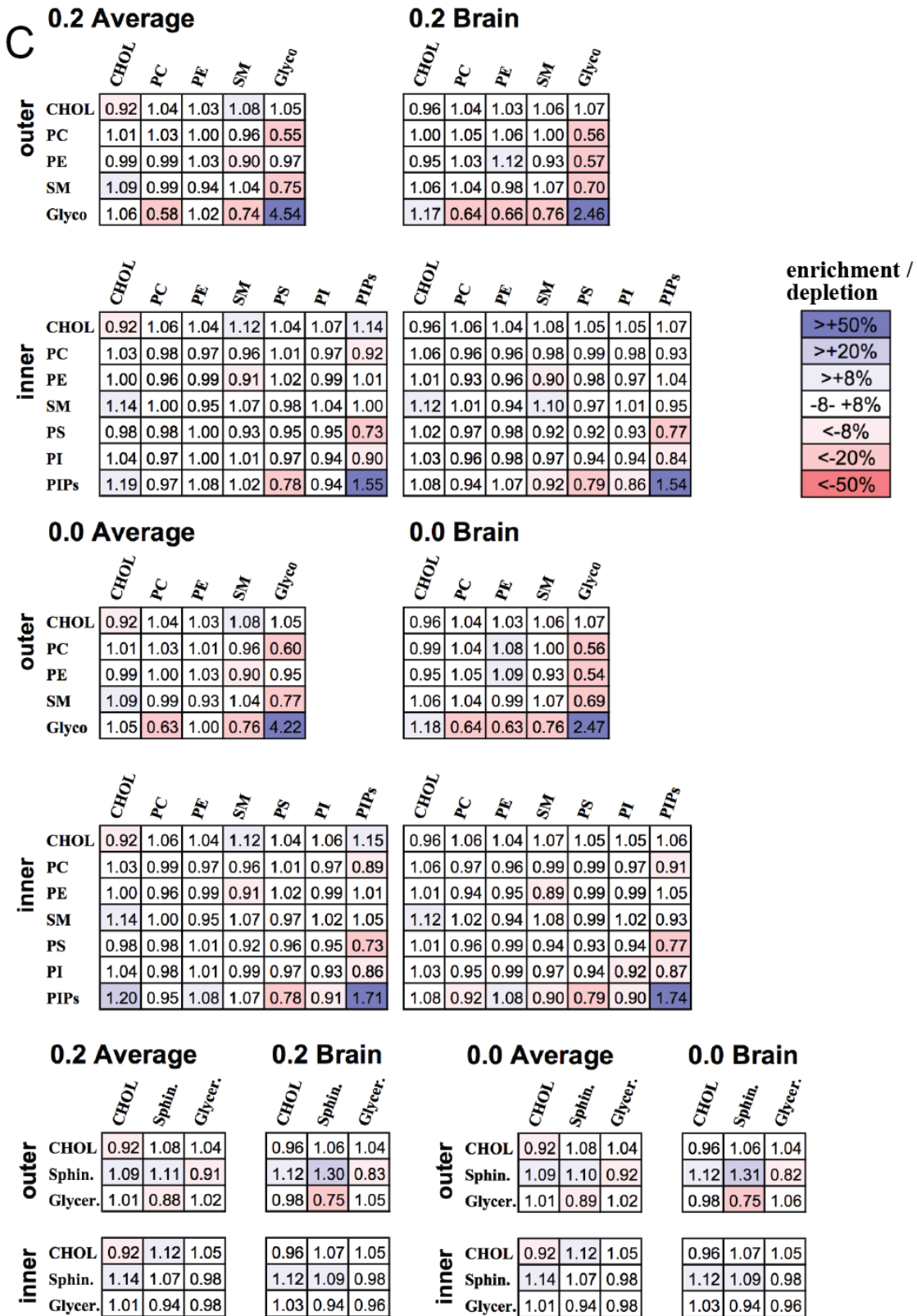


Figure S6. Bilayer undulation simulations. Starting from the main **Brain** and **Average PM** simulations at 75 μs , simulations were run for 5 μs with either tenfold weaker, or no restraints on bilayer undulations (0.2 and 0.0 $\text{kJ mol}^{-1} \text{nm}^{-2}$, respectively), see also Fig. 4. (A) Outer leaflet top view snapshots of the final structure of each simulation are shown. The lipids are colored in the same way as in Fig. 1 and S1. The deviations of the bilayer normal away from the box z-axes (white to red in degrees) are shown on top of the fitted bilayer surfaces. (B) Size histograms of cholesterol enriched domains in the outer leaflet of each simulation, using the threshold that maximizes the number of domains. The histograms were made from 2 μs simulation blocks ranging from the beginning to the end the simulations (75 – 80 μs for the main simulations). (C) Number of neighboring lipids (within 1.5 nm) grouped by headgroup type (top) and linker type (bottom); where Sphin. are sphingolipids and Glycer. are glycerolipids. Values are averaged over the last 2 μs of the simulation and normalized to the weighted average number of neighbors of each type to highlight the relative enrichment/depletion of those lipids. Standard errors for all counts are <0.03 . Value for the main simulations, with 2.0 $\text{kJ mol}^{-1} \text{nm}^{-2}$ undulation restraints are in Fig. S2.

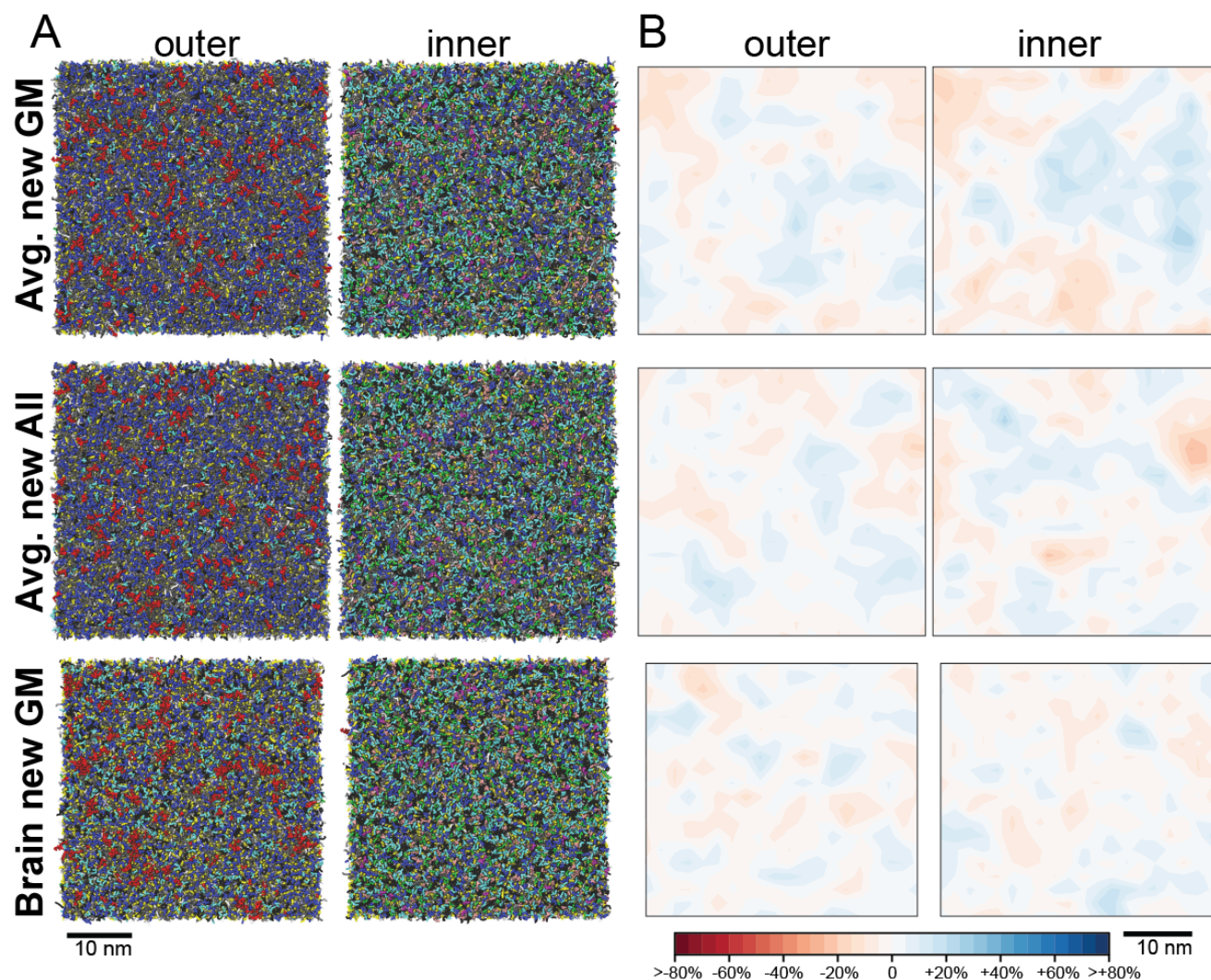


Figure S7. Alternative lipid parameters. Smaller repeat simulations ($\sim 6,000$ lipids) were run for $50 \mu\text{s}$ with the recently published alternative parameters for GM1 and GM3 (30) (**Avg. new GM** and **Brain new GM**) as well as an **Average** PM mixture with the all the most up-to-date Martini parameters (**Avg. new All**), see Supplementary Methods. (A) Snapshots of the outer/inner leaflet of the simulations after $50 \mu\text{s}$ are shown using the same color scheme as in Fig. 1. (B) 2D density maps averaged over the last 200 ns are shown for cholesterol's ROH beads in the inner/outer leaflet of each simulations. Average properties including lipid flip-flop rates were also calculated for these control simulations and were similar as their corresponding **Average** or **Brain** larger simulations. Only CHOL, DAG, and CER lipids flip-flopped and their rates are: CHOL $7.30 \pm 0.07 \times 10^6 \text{ s}^{-1}$, DAG $6.2 \pm 0.2 \times 10^6 \text{ s}^{-1}$, and CER $1.5 \pm 0.4 \times 10^4 \text{ s}^{-1}$ (**Avg. new GM**); CHOL $7.79 \pm 0.07 \times 10^6 \text{ s}^{-1}$, DAG $3.5 \pm 0.1 \times 10^6 \text{ s}^{-1}$, and CER $1.5 \pm 0.4 \times 10^4 \text{ s}^{-1}$ (**Avg. new All**); and CHOL $4.84 \pm 0.02 \times 10^6 \text{ s}^{-1}$, DAG $2.8 \pm 0.1 \times 10^6 \text{ s}^{-1}$, and CER $2 \pm 1 \times 10^4 \text{ s}^{-1}$ (**Brain new GM**).

Table S1 Lipid composition^a

Lipid tail sn-1	Lipid tail sn-2	Acronym	Average				Brain			
			Outer leaflet count	Outer leaflet mole fraction	Inner leaflet count	Inner leaflet mole fraction	Outer leaflet count	Outer leaflet mole fraction	Inner leaflet count	Inner leaflet mole fraction
Phosphatidylcholine - PC			<i>outer/inner ratio</i>		0.69	0.31			0.65	0.35
CCCC	CCCC	DPPC					531	0.053	284	0.030
CCCC	CDCC	POPC	1205	0.122	550	0.059	868	0.087	463	0.049
CDCC	CDCC	DOPC	106	0.011	49	0.005	221	0.022	118	0.012
CCCC	CDDC	PIPC	1772	0.179	810	0.087				
CCCC	CDDD	PFPC					59	0.006	32	0.003
CCCC	CDDCC	PEPC	71	0.007	32	0.003				
CCCC	DDDDC	PAPC	283	0.029	129	0.014	463	0.046	247	0.026
DDDDC	DDDDC	DAPC	35	0.004	16	0.002				
CCCC	DDDDDC	PUPC	71	0.007	32	0.003	169	0.017	90	0.010
CDCC	CDDC	OIPC					59	0.006	32	0.003
CDCC	DDDDDC	OUPC					42	0.004	22	0.002
Total:			3543	0.357	1618	0.173	2412	0.242	1288	0.136
Phosphatidylethanolamine - PE			<i>outer/inner ratio</i>		0.19	0.81			0.35	0.65
CCCC	CCDC	POPE	135	0.014	569	0.061	127	0.013	234	0.025
CDCC	CDCC	DOPE	44	0.004	190	0.020				
CCCC	CDDC	PIPE	90	0.009	380	0.041				
CCCC	CDDDC	PQPE	22	0.002	95	0.010				
CCCC	DDDDC	PAPE	124	0.013	522	0.056	312	0.031	574	0.061
DDDDC	DDDDC	DAPE	78	0.008	332	0.036				
CCCC	DDDDDC	PUPE	44	0.004	190	0.020	500	0.050	922	0.097
DDDDDC	DDDDDC	DUPE	22	0.002	95	0.010				
CDCC	CDDC	OIPE					14	0.001	27	0.003
CDCC	DDDDC	OAPE					68	0.007	127	0.013
CDCC	DDDDDC	OUPPE					72	0.007	133	0.014
Total:			559	0.056	2373	0.254	1093	0.110	2017	0.213
Sphingomyelin - SM			<i>outer/inner ratio</i>		0.69	0.31		0.80		0.20
TCC	CCCC	DPSM	611	0.062	279	0.030	581	0.058	143	0.015
TCCC	CCCCC	DBSM	133	0.013	61	0.007				
TCCCC	CCCCCC	DXSM	247	0.025	113	0.012				
TCC	CDCC	POSM	38	0.004	17	0.002	71	0.007	17	0.002
TCC	CCDCC	PGSM	38	0.004	17	0.002				
TCC	CCCDCC	PNSM	381	0.038	174	0.019	132	0.013	32	0.003
TCC	CCCCC	PBSM					108	0.011	27	0.003
TCCC	CCCDCC	BNSM	191	0.019	86	0.009				
TCCCC	CCCDCC	XNSM	267	0.027	121	0.013				
Total:			1906	0.192	868	0.093	892	0.089	219	0.023
Phosphatidylserine - PS			<i>outer/inner ratio</i>		0.00	1.00			0.00	1.00
CCCC	CCCC	DPPS							46	0.005
CCCC	CDCC	POPS			200	0.021			232	0.025

CCCC	CDDC	PIPS		79	0.008			
CCCC	CDDDC	PQPS		39	0.004			
CCCC	DDDDC	PAPS		461	0.049		261	0.028
DDDDC	DDDDC	DAPS		20	0.002			
CCCC	DDDDDC	PUPS		180	0.019		326	0.034
DDDDDC	DDDDDC	DUPS		20	0.002			
CDCC	DDDDDC	OUPS					65	0.007
Total:				999	0.107		930	0.098
Glycolipid - GM1			<i>outer/inner ratio</i>	1.00	0.00		1.00	0.00
TCC	CCCC	DPG1	89	0.009		89	0.009	
TCCC	CCCCC	DBG1				16	0.002	
TCCCC	CCCCCC	DXG1	51	0.005				
TCC	CDCC	POG1				10	0.001	
TCC	CCCDCC	PNG1	64	0.006		20	0.002	
TCCCC	CCCDCC	XNG1	51	0.005				
Total:			255	0.026		135	0.014	
Glycolipid - GM3			<i>outer/inner ratio</i>	1.00	0.00		1.00	0.00
TCC	CCCC	DPG3	89	0.009		89	0.009	
TCCC	CCCCC	DBG3				16	0.002	
TCCCC	CCCCCC	DXG3	51	0.005				
TCC	CDCC	POG3				10	0.001	
TCC	CCCDCC	PNG3	64	0.006		20	0.002	
TCCCC	CCCDCC	XNG3	51	0.005				
Total:			255	0.026		135	0.014	
Cerebrosides			<i>outer/inner ratio</i>				1.00	0.00
TCC	CCCC	DPGS				484	0.049	
TCCC	CCCCC	DBGS				90	0.009	
TCC	CDCC	POGS				59	0.006	
TCC	CCCDCC	PNGS				109	0.011	
Total:						742	0.074	
Phosphatidylinositol - PI			<i>outer/inner ratio</i>	0.00	1.00		0.00	1.00
CCCC	CDCC	POPI		137	0.015		121	0.013
CCCC	CDDC	PIPI		120	0.013		48	0.005
CCCC	DDDDC	PAPI		120	0.013		121	0.013
CCCC	DDDDDC	PUPI		51	0.005		194	0.020
Total:				428	0.046		484	0.051
Phosphatidic acid - PA			<i>outer/inner ratio</i>	0.00	1.00		0.00	1.00
CCCC	CDCC	POPA		46	0.005		13	0.001
CCCC	CDDC	PIPA		39	0.004			
CCCC	DDDDC	PAPA		39	0.004		25	0.003
CCCC	DDDDDC	PUPA		17	0.002			
Total:				141	0.015		38	0.004
Phosphatidylinositol phosphates - PIPs			<i>outer/inner ratio</i>	0.00	1.00		0.00	1.00
CCCC	CDCC	POP1		48	0.005		15	0.002
CCCC	DDDDC	PAP1					29	0.003
CCCC	CDCC	POP2		48	0.005		15	0.002
CCCC	DDDDC	PAP2					29	0.003
CCCC	CDCC	POP3		48	0.005		15	0.002
CCCC	DDDDC	PAP3					29	0.003
Total:				144	0.015		132	0.014
Ceramide - CER			<i>outer/inner ratio</i>	0.65	0.35		0.50	0.50

TCC	CCCC	DPCE	30	0.003	16	0.002	38	0.004	37	0.004
TCCC	CCCCC	DBCE					6	0.001	6	0.001
TCCCC	CCCCCC	DXCE	17	0.002	9	0.001				
TCC	CCCDCC	FNCE	20	0.002	12	0.001	8	0.001	8	0.001
TCC	CDCC	POCE					4	0.000	4	0.000
TCCCC	CCCDCC	XNCE	17	0.002	9	0.001				
		Total:	84	0.008	46	0.005	56	0.006	55	0.006
Lysophosphatidylcholine - LPC			<i>outer/inner ratio</i>		1.00	0.00			0.67	0.33
CCCC		PPC	64	0.006			20	0.002	10	0.001
CDCC		OPC	20	0.002						
CDDC		IPC	18	0.002			10	0.001	5	0.001
DDDDC		APC	18	0.002						
DDDDDC		UPC	7	0.001						
		Total:	127	0.013			30	0.003	15	0.002
Lysophosphatidylethanolamine – LPE			<i>outer/inner ratio</i>						0.33	0.67
CCCC		PPE					5	0.001	10	0.001
CDDC		IPE					10	0.001	20	0.002
		Total:					15	0.002	30	0.003
Diacylglycerol - DAG			<i>outer/inner ratio</i>		0.60	0.40			0.50	0.50
CCCC	CDCC	PODG	25	0.003	17	0.002	13	0.001	13	0.001
CCCC	CDDC	PIDG	23	0.002	15	0.002				
CCCC	DDDDC	PADG	23	0.002	15	0.002	25	0.003	25	0.003
CCCC	DDDDDC	PUDG	9	0.001	6	0.001				
		Total:	80	0.008	53	0.006	38	0.004	38	0.004
Cholesterol - CHOL			<i>outer/inner ratio</i>		0.54	0.46			0.51	0.49
		CHOL	3104	0.313	2656	0.285	4431	0.444	4222	0.446
Total all lipids			9913	1.000	9326	1.000	9979	1.000	9468	1.000

^aRelative abundance of the different lipid species in the plasma membrane leaflets as well as the ratio between the leaflets. On the microsecond time scale lipids with a “proper” hydrated headgroups do not flip-flop between the leaflets and their number in each leaflet is constant. In contrast cholesterol (CHOL), ceramides (CER) and diacylglycerols (DAG) do flip-flop; therefore, their average numbers fluctuate somewhat over the simulations. The numbers reported here are initial values. Averaged over the last 10 μ s of the simulations the total outer/inner leaflet counts are: CHOL 3152/2608, CER 83/47, DAG 83/50 in the **Average** and CHOL 4412/4241, CER 53/58, DAG 29/47 in the **Brain**. The Martini beads for each lipid tail are listed: C beads represent a saturated carbon chain, D beads have 1-2 cis double bonds, and T beads are below the AM1 sphingosine linker with the trans double bound. Note, the Martini O tail (representing oleic acid or palmitoleic acid) used to be CCDC but now is CDCC. The old arrangement is used in the **Average** mixture for consistency with (1).

Table S2 Lipid average order parameter^a

Lipid tail sn-1	Lipid tail sn-2	Acronym	Average						Brain						
			Inner leaflet count	Inner tail sn-1	Inner tail sn-2	Outer leaflet count	Outer tail sn-1	Outer tail sn-2	Inner leaflet count	Inner tail sn-1	Inner tail sn-2	Outer leaflet count	Outer tail sn-1	Outer tail sn-2	
Phosphatidylcholine - PC															
CCCC	CCCC	DPPC								284	0.482	0.506	531	0.536	0.553
CCCC	CDCC	POPC	550	0.475	0.440	1205	0.478	0.444	463	0.458	0.408	868	0.511	0.447	
CDCC	CDCC	DOPC	49	0.417	0.434	106	0.415	0.434	118	0.371	0.395	221	0.412	0.429	
CCCC	CDDC	PIPC	810	0.459	0.260	1772	0.458	0.253							
CCCC	CDDD	PFPC							32	0.459	0.183	59	0.499	0.167	
CCCC	CDDCC	PEPC	32	0.463	0.283	71	0.458	0.274							
CCCC	DDDDC	PAPC	129	0.455	0.131	283	0.454	0.119	247	0.448	0.139	463	0.497	0.136	
DDDDC	DDDDC	DAPC	16	0.123	0.153	35	0.108	0.137							
CCCC	DDDDDC	PUPC	32	0.455	0.112	71	0.444	0.103	90	0.456	0.076	169	0.495	0.063	
CDCC	CDDC	OIPC							32	0.368	0.269	59	0.407	0.272	
CDCC	DDDDDC	OUPC							22	0.370	0.075	42	0.398	0.058	
Phosphatidylethanolamine - PE															
CCCC	CCDC	POPE	569	0.471	0.439	135	0.471	0.441	234	0.448	0.403	127	0.505	0.445	
CDCC	CDCC	DOPE	190	0.412	0.431	44	0.415	0.434							
CCCC	CDDC	PIPE	380	0.452	0.267	90	0.454	0.261							
CCCC	CDDDC	PQPE	95	0.446	0.209	22	0.458	0.213							
CCCC	DDDDC	PAPE	522	0.449	0.130	124	0.446	0.121	574	0.442	0.136	312	0.491	0.135	
DDDDC	DDDDC	DAPE	332	0.123	0.150	78	0.110	0.138							
CCCC	DDDDDC	PUPE	190	0.445	0.110	44	0.442	0.104	922	0.443	0.075	500	0.490	0.063	
DDDDDC	DDDDDC	DUPE	95	0.105	0.127	22	0.091	0.117							
CDCC	CDDC	OIPE							27	0.369	0.271	14	0.401	0.277	
CDCC	DDDDC	OAPE							127	0.359	0.133	68	0.394	0.132	
CDCC	DDDDDC	OUPE							133	0.362	0.075	72	0.393	0.066	
Sphingomyelin - SM															
TCC	CCCC	DPSM	279	0.522	0.552	611	0.529	0.564	143	0.515	0.574	581	0.565	0.611	
TCCC	CCCCC	DBSM	61	0.464	0.536	133	0.470	0.545							
TCCCC	CCCCC	DXSM	113	0.393	0.483	247	0.397	0.490							
TCC	CDCC	POSM	17	0.451	0.544	38	0.453	0.547	17	0.426	0.555	71	0.457	0.581	
TCC	CCDCC	PGSM	17	0.390	0.533	38	0.404	0.557							
TCC	CCCDCC	PNSM	174	0.355	0.553	381	0.358	0.559	32	0.341	0.571	132	0.385	0.605	
TCC	CCCCC	PBSM							27	0.443	0.576	108	0.497	0.610	
TCCC	CCCDCC	BNSM	86	0.354	0.530	191	0.357	0.536							
TCCCC	CCCDCC	XNSM	121	0.360	0.478	267	0.363	0.483							
Phosphatidylserine - PS															
CCCC	CCCC	DPPS							46	0.488	0.507				
CCCC	CDCC	POPS	200	0.474	0.442				232	0.458	0.410				
CCCC	CDDC	PIPS	79	0.461	0.265										
CCCC	CDDDC	PQPS	39	0.462	0.214										
CCCC	DDDDC	PAPS	461	0.455	0.133				261	0.451	0.140				

DDDDC	APC					18	0.150							
DDDDDC	UPC					7	0.121							
Lysophosphatidylethanolamine – LPE														
CCCC	PPE								10	0.487		5	0.544	
CDDC	IPE								20	0.289		10	0.304	
Diacylglycerol - DAG														
CCCC	CDCC	PODG	17	0.435	0.390	25	0.435	0.390	13	0.456	0.385	13	0.456	0.385
CCCC	CDDC	PIDG	15	0.412	0.215	23	0.412	0.215						
CCCC	DDDDC	PADG	15	0.401	0.091	23	0.401	0.091	25	0.438	0.105	25	0.438	0.105
CCCC	DDDDDC	PUDG	6	0.414	0.073	9	0.414	0.073						

^aLipid tail order parameters (S) were calculated for each lipid type as explained in the SI methods. Here we show the absolute average order parameter per tail in each leaflet. ^bDAG and CER lipids flip-flop between the leaflets, therefore, their tail order was determined jointly in both leaflets. Standard errors were calculated using block averaging; they were typically ~ 0.003 and all were less than 0.015, therefore, skipped for brevity. The weighted average tail order over all lipid types (excluding lipids that flip-flop) are: **Average** [0.435,0.374] / [0.430,0.301] and **Brain** [0.487,0.391] / [0.444,0.224], respectively for the [sn-1, sn-2] tails in the outer/inner leaflet.

Table S3 Lipid diffusion rates^a

Acronym	Average						Brain					
	Outer leaflet count	Outer diffusion avg. / 10^{-7} cm ² /s	Outer diffusion error / 10^{-7} cm ² /s	Inner leaflet count	Inner diffusion avg. / 10^{-7} cm ² /s	Inner diffusion error / 10^{-7} cm ² /s	Outer leaflet count	Outer diffusion avg. / 10^{-7} cm ² /s	Outer diffusion error / 10^{-7} cm ² /s	Inner leaflet count	Inner diffusion avg. / 10^{-7} cm ² /s	Inner diffusion error / 10^{-7} cm ² /s
Phosphatidylcholine - PC												
DPPC							531	1.48	0.27	284	2.59	0.15
POPC	1205	3.41	0.24	550	4.42	0.25	868	1.76	0.07	463	2.96	0.17
DOPC	106	3.46	0.43	49	3.62	0.16	221	1.79	0.17	118	2.61	0.22
PIPC	1772	3.63	0.23	810	4.58	0.11						
PFPC							59	2.26	0.19	32	3.53	0.06
PEPC	71	2.89	0.69	32	4.31	0.96						
PAPC	283	3.21	0.11	129	5.25	0.34	463	1.98	0.17	247	2.65	0.41
DAPC	35	3.06	0.21	16	4.44	2.60						
PUPC	71	3.22	0.79	32	3.93	0.25	169	2.27	0.06	90	3.02	0.62
OIPC							59	1.81	0.01	32	2.42	0.14
OUPC							42	2.31	0.44	22	1.98	1.67
Phosphatidylethanolamine - PE												
POPE	135	2.64	0.25	569	4.05	0.02	127	1.54	0.18	234	2.31	0.02
DOPE	44	2.80	0.67	190	4.10	0.48						
PIPE	90	3.35	0.19	380	4.20	0.16						
PQPE	22	2.70	0.46	95	4.60	0.57						
PAPE	124	3.24	0.06	522	4.42	0.21	312	1.96	0.23	574	2.97	0.01
DAPE	78	3.74	0.07	332	5.02	0.03						
PUPE	44	3.83	0.68	190	4.57	0.73	500	1.88	0.11	922	2.80	0.04
DUPE	22	4.35	0.98	95	4.39	0.24						
OIPE							14	1.40	0.10	27	2.74	0.55
OAPE							68	2.39	0.01	127	2.81	0.25
OUPE							72	2.25	0.53	133	3.34	0.04
Sphingomyelin - SM												
DPSM	611	3.33	0.18	279	4.24	0.59	581	1.62	0.02	143	2.48	0.04
DBSM	133	2.33	0.54	61	4.42	0.97						
DXSM	247	2.44	0.11	113	3.62	0.17						
POSM	38	3.80	0.99	17	2.49	0.27	71	1.61	0.12	17	1.88	0.80
PGSM	38	3.81	0.60	17	6.94	2.31						
PNSM	381	2.92	0.05	174	3.81	0.09	132	1.53	0.04	32	2.19	0.35
PBSM							108	1.53	0.66	27	1.32	0.89
BNSM	191	2.83	0.08	86	4.03	0.62						
XNSM	267	2.98	0.16	121	3.73	0.03						
Phosphatidylserine - PS												
DPPS										46	2.44	0.26
POPS				200	4.47	0.12				232	2.76	0.09
PIPS				79	5.13	0.54						
PQPS				39	4.06	0.23						
PAPS				461	4.53	0.33				261	3.19	0.13

DAPS				20	3.74	0.23						
PUPS				180	4.21	0.53		326	2.98	0.06		
DUPS				20	2.62	0.14						
OUPS								65	2.87	0.09		
Glycolipid - GM1												
DPG1	89	1.34	0.27				89	0.74	0.05			
DBG1							16	0.49	0.19			
DXG1	51	1.10	0.20									
POG1							10	0.78	0.12			
PNG1	64	1.11	0.45				20	0.81	0.35			
XNG1	51	1.04	0.22									
Glycolipid - GM3												
DPG3	89	1.86	0.74				89	0.88	0.06			
DBG3							16	0.56	0.02			
DXG3	51	1.45	0.05									
POG3							10	0.42	0.38			
PNG3	64	2.10	0.70				20	1.20	0.46			
XNG3	51	2.04	0.85									
Cerebrosides												
DPGS							484	0.98	0.13			
DBGS							90	0.94	0.28			
POGS							59	0.79	0.35			
PNGS							109	1.06	0.01			
Phosphatidylinositol - PI												
POPI				137	4.40	0.29		121	2.59	0.08		
PIPI				120	4.54	0.65		48	3.34	0.82		
PAPI				120	5.08	0.28		121	2.98	0.09		
PUPI				51	4.08	1.37		194	2.80	0.74		
Phosphatidic acid - PA												
POPA				46	4.06	0.35		13	2.65	1.18		
PIPA				39	3.93	0.39						
PAPA				39	2.97	0.51		25	1.75	1.84		
PUPA				17	3.27	2.06						
Phosphatidylinositol phosphates - PIPs												
POP1				48	3.82	0.09		15	2.52	0.73		
PAP1								29	2.95	0.66		
POP2				48	4.26	0.31		15	2.09	0.02		
PAP2								29	2.00	0.17		
POP3				48	3.36	0.64		15	1.67	0.50		
PAP3								29	2.56	0.29		
Ceramide - CER^b												
DPCE	30	5.78	1.47	16	5.78	1.47	38	2.35	0.16	37	2.35	0.16
DBCE							6	2.06	0.77	6	2.06	0.77
DXCE	17	4.13	0.50	9	4.13	0.50						
PNCE	20	4.44	1.24	12	4.44	1.24	8	1.69	0.35	8	1.69	0.35
POCE							4	4.63	1.15	4	4.63	1.15
XNCE	17	2.15	0.05	9	2.15	0.05						
Lysophosphatidylcholine - LPC												
PPC	64						20	1.87	0.68	10	6.67	0.46
OPC	20											
IPC	18						10	2.37	1.28	5	4.67	3.68

APC	18											
UPC	7											
Lysophosphatidylethanolamine – LPE												
PPE							5	1.29	0.17	10	2.98	0.91
IPE							10	1.64	0.77	20	4.52	0.02
Diacylglycerol - DAG^b												
PODG	25	5.65	2.28	17	5.65	2.28	13	2.18	0.05	13	2.18	0.05
PIDG	23	6.54	1.55	15	6.54	1.55						
PADG	23	5.86	1.10	15	5.86	1.10	25	3.89	0.76	25	3.89	0.76
PUDG	9	4.05	0.06	6	4.05	0.06						
Cholesterol - CHOL^b												
CHOL	3104	4.99	0.11	2656	4.99	0.11	4431	3.02	0.12	4222	3.02	0.12

^aLipid lateral diffusion was evaluated for each lipid type from the lipids' MSD in the membrane plane, see SI methods. ^bCHOL, DAG, and CER lipids flip-flop between the leaflets, therefore, their diffusion was determined jointly in both leaflets. The weighted average diffusion rates in the outer/inner leaflet (excluding lipids that flip-flop) are: **Average** 3.1 ± 0.3 / 4.3 ± 0.3 and **Brain** 1.6 ± 0.2 / 2.8 ± 0.2 in 10^{-7} cm²/s.

Supporting References:

1. Ingólfsson, H.I., M.N. Melo, F.J. van Eerden, C. Arnarez, C.A. Lopez, T.A. Wassenaar, X. Periole, A.H. De Vries, D.P. Tieleman, and S.J. Marrink. 2014. Lipid Organization of the Plasma Membrane. *J. Am. Chem. Soc.* 136: 14554–14559.
2. O'Brien, J.S., and E.L. Sampson. 1965. Lipid composition of the normal human brain: gray matter, white matter, and myelin. *J. Lipid Res.* 6: 537–544.
3. Kishimoto, Y., B.W. Agranoff, N.S. Radin, and R.M. Burton. 1969. Comparison of the fatty acids of lipids of subcellular brain fractions. *Journal of Neurochemistry.* 16: 397–404.
4. Breckenridge, W.C., G. Gombos, and I.G. Morgan. 1972. The lipid composition of adult rat brain synaptosomal plasma membranes. *BBA - Biomembranes.* 266: 695–707.
5. Christie, W.W. 1985. Rapid separation and quantification of lipid classes by high performance liquid chromatography and mass (light-scattering) detection. *J. Lipid Res.* 26: 507–512.
6. Abbott, S.K., P.L. Else, T.A. Atkins, and A.J. Hulbert. 2012. Fatty acid composition of membrane bilayers: Importance of diet polyunsaturated fat balance. *BBA - Biomembranes.* 1818: 1309–1317.
7. Atilla-Gokcumen, G.E., E. Muro, J. Relat-Goberna, S. Sasse, A. Bedigian, M.L. Coughlin, S. Garcia-Manyes, and U.S. Eggert. 2014. Dividing Cells Regulate Their Lipid Composition and Localization. *Cell.* 156: 428–439.
8. Levental, K.R., J.H. Lorent, X. Lin, A.D. Skinkle, M.A. Surma, E.A. Stockenbojer, A.A. Gorfe, and I. Levental. 2016. Polyunsaturated Lipids Regulate Membrane Domain Stability by Tuning Membrane Order. *Biophys. J.* 110: 1800–1810.
9. Tulodziecka, K., B.B. Diaz-Rohrer, M.M. Farley, R.B. Chan, G. Di Paolo, K.R. Levental, M.N. Waxham, and I. Levental. 2016. Remodeling of the postsynaptic plasma membrane during neural development. *Mol. Biol. Cell.* 27: 3480–3489.
10. van Meer, G. 2005. Cellular lipidomics. *EMBO J.* 24: 3159–3165.
11. Fernandez, C., M. Sandin, J.L. Sampaio, P. Almgren, K. Narkiewicz, M. Hoffmann, T. Hedner, B. Wahlstrand, K. Simons, A. Shevchenko, P. James, and O. Melander. 2013. Plasma Lipid Composition and Risk of Developing Cardiovascular Disease. *PLoS ONE.* 8: e71846.
12. Holthuis, J.C.M., and A.K. Menon. 2014. Lipid landscapes and pipelines in membrane homeostasis. *Nature.* 510: 48–57.
13. Wells, M.A., and J.C. Dittmer. 1967. A comprehensive study of the postnatal changes in the concentration of the lipids of developing rat brain. *Biochemistry.* 6: 3169–3175.

14. Lutzke, B.S., and J.M. Braughler. 1990. An Improved Method for the Identification and Quantitation of Biological Lipids by Hplc Using Laser Light-Scattering Detection. *J. Lipid Res.* 31: 2127–2130.
15. Kracun, I., H. Rosner, V. Drnovsek, M. Heffer-Lauc, C. Cosović, and G. Lauc. 1991. Human brain gangliosides in development, aging and disease. *Int. J. Dev. Biol.* 35: 289–295.
16. Diagne, A., J. Fauvel, M. Record, H. Chap, and L. Douste-Blazy. 1984. Studies on ether phospholipids. II. Comparative composition of various tissues from human, rat and guinea pig. *Biochim. Biophys. Acta.* 793: 221–231.
17. Homan, R., and M.K. Anderson. 1998. Rapid separation and quantitation of combined neutral and polar lipid classes by high-performance liquid chromatography and evaporative light-scattering mass detection. *J. Chromatogr. B Biomed. Sci. Appl.* 708: 21–26.
18. Han, X., D.M. Holtzman, and D.W. McKeel. 2001. Plasmalogen deficiency in early Alzheimer's disease subjects and in animal models: molecular characterization using electrospray ionization mass spectrometry. *J. Neurochem.* 77: 1168–1180.
19. Han, X., and R.W. Gross. 2005. Shotgun lipidomics: Electrospray ionization mass spectrometric analysis and quantitation of cellular lipidomes directly from crude extracts of biological samples. *Mass Spectrom. Rev.* 24: 367–412.
20. Sharon, R., I. Bar-Joseph, G.E. Mirick, C.N. Serhan, and D.J. Selkoe. 2003. Altered Fatty Acid Composition of Dopaminergic Neurons Expressing α -Synuclein and Human Brains with α -Synucleinopathies. *J. Biol. Chem.* 278: 49874–49881.
21. Chan, R.B., T.G. Oliveira, E.P. Cortes, L.S. Honig, K.E. Duff, S.A. Small, M.R. Wenk, G. Shui, and G. Di Paolo. 2012. Comparative lipidomic analysis of mouse and human brain with Alzheimer disease. *J. Biol. Chem.* 287: 2678–2688.
22. Lam, S.M., Y. Wang, X. Duan, M.R. Wenk, R.N. Kalaria, C.P. Chen, M.K.P. Lai, and G. Shui. 2014. The brain lipidomes of subcortical ischemic vascular dementia and mixed dementia. *Neurobiol. Aging.* 35: 2369–2381.
23. Arai, Y., J.L. Sampaio, M. Wilsch-Bräuninger, A.W. Ettinger, C. Haffner, and W.B. Huttner. 2015. Lipidome of midbody released from neural stem and progenitor cells during mammalian cortical neurogenesis. *Front. Cell. Neurosci.* 9: 428–411.
24. Oliveira, T.G., R.B. Chan, F.V. Bravo, A. Miranda, R.R. Silva, B. Zhou, F. Marques, V. Pinto, J.J. Cerqueira, G. Di Paolo, and N. Sousa. 2015. The impact of chronic stress on the rat brain lipidome. *Mol. Psychiatry.* 21: 80–88.
25. Shevchenko, A., and K. Simons. 2010. Lipidomics: coming to grips with lipid diversity. *Nat. Rev. Mol. Cell Biol.* 11: 593–598.
26. Clark, J., K.E. Anderson, V. Juvin, T.S. Smith, F. Karpe, M.J.O. Wakelam, L.R. Stephens,

- and P.T. Hawkins. 2011. Quantification of PtdInsP3 molecular species in cells and tissues by mass spectrometry. *Nat. Meth.* 8: 267–272.
27. Marrink, S.J., A.H. De Vries, and A.E. Mark. 2004. Coarse grained model for semiquantitative lipid simulations. *J. Phys. Chem. B.* 108: 750–760.
 28. Marrink, S.J., H.J. Risselada, S. Yefimov, D.P. Tieleman, and A.H. De Vries. 2007. The MARTINI force field: coarse grained model for biomolecular simulations. *J. Phys. Chem. B.* 111: 7812–7824.
 29. Wassenaar, T.A., H.I. Ingólfsson, R.A. Böckmann, D.P. Tieleman, and S.J. Marrink. 2015. Computational Lipidomics with insane: A Versatile Tool for Generating Custom Membranes for Molecular Simulations. *J. Chem. Theory Comput.* 11: 2144–2155.
 30. Gu, R.-X., H.I. Ingólfsson, A.H. De Vries, S.J. Marrink, and D.P. Tieleman. 2017. Ganglioside-Lipid and Ganglioside-Protein Interactions Revealed by Coarse-Grained and Atomistic Molecular Dynamics Simulations. *J. Phys. Chem. B.* 121: 3262–3275.
 31. Lopez, C.A., Z. Sovova, F.J. van Eerden, A.H. De Vries, and S.J. Marrink. 2013. Martini force field parameters for glycolipids. *J. Chem. Theory Comput.* 9: 1694–1708.
 32. Pronk, S., S. Páll, R. Schulz, P. Larsson, P. Bjelkmar, R. Apostolov, M.R. Shirts, J.C. Smith, P.M. Kasson, D. van der Spoel, B. Hess, and E. Lindahl. 2013. GROMACS 4.5: a high-throughput and highly parallel open source molecular simulation toolkit. *Bioinformatics.* 29: 845–854.
 33. de Jong, D.H., S. Baoukina, H.I. Ingólfsson, and S.J. Marrink. 2016. Martini straight: Boosting performance using a shorter cutoff and GPUs. *Comput. Phys. Commun.* 199: 1–7.
 34. Bussi, G., D. Donadio, and M. Parrinello. 2007. Canonical sampling through velocity rescaling. *J. Chem. Phys.* 126: 014101.
 35. Parrinello, M., and A. Rahman. 1981. Polymorphic transitions in single crystals: A new molecular dynamics method. *J. Appl. Phys.* 52: 7182–7190.
 36. Michaud-Agrawal, N., E.J. Denning, T.B. Woolf, and O. Beckstein. 2011. MDAAnalysis: A toolkit for the analysis of molecular dynamics simulations. *J. Comput. Chem.* 32: 2319–2327.
 37. Xie, H., K.T. McDonnell, and H. Qin. 2004. *Surface Reconstruction of Noisy and Defective Data Sets*. Washington, DC, USA: IEEE Computer Society. pp. 259–266.
 38. Kazhdan, M., M. Bolitho, and H. Hoppe. 2006. *Poisson Surface Reconstruction*. Aire-la-Ville, Switzerland, Switzerland: Eurographics Association. pp. 61–70.
 39. Floater, M.S., and K. Hormann. 2005. *Surface Parameterization: a Tutorial and Survey*. In: Dodgson NA, MS Floater, MA Sabin, editors. *Advances in Multiresolution for Geometric Modelling*. Berlin, Heidelberg: Springer Berlin Heidelberg. pp. 157–186.

40. Venable, R.M., H.I. Ingólfsson, M.G. Lerner, B.S. Perrin, B.A. Camley, S.J. Marrink, F.L.H. Brown, and R.W. Pastor. 2017. Lipid and Peptide Diffusion in Bilayers: The Saffman-Delbrück Model and Periodic Boundary Conditions. *J. Phys. Chem. B.* 121: 3443–3457.
41. Castillo, N., L. Monticelli, J. Barnoud, and D.P. Tieleman. 2013. Free energy of WALP23 dimer association in DMPC, DPPC, and DOPC bilayers. *Chem. Phys. Lipids.* 169: 95–105.
42. Chavent, M., T. Reddy, J. Goose, A.C.E. Dahl, J.E. Stone, B. Jobard, and M.S.P. Sansom. 2014. Methodologies for the analysis of instantaneous lipid diffusion in md simulations of large membrane systems. *Faraday Discuss.* 169: 455–475.
43. Bremer, P.-T., G.H. Weber, V. Pascucci, M. Day, and J.B. Bell. 2010. Analyzing and tracking burning structures in lean premixed hydrogen flames. *IEEE Trans. Vis. Comput. Graph.* 16: 248–260.
44. Bennett, J.C., V. Krishnamoorthy, S. Liu, R.W. Grout, E.R. Hawkes, J.H. Chen, J. Shepherd, V. Pascucci, and P.-T. Bremer. 2011. Feature-based statistical analysis of combustion simulation data. *IEEE Trans. Vis. Comput. Graph.* 17: 1822–1831.